Amyloid-β Fibrillogenesis Seeded by Interface-Induced Peptide Misfolding and Self-Assembly

Eva Y. Chi,[†] Shelli L. Frey,[‡] Amy Winans,[§] Kin Lok H. Lam,[¶] Kristian Kjaer,[‖] Jaroslaw Majewski,[††] and Ka Yee C. Lee[§*]

[†]Department of Chemical and Nuclear Engineering, Center for Biomedical Engineering, University of New Mexico, Albuquerque, New Mexico; [‡]Department of Chemistry, Gettysburg College, Gettysburg, Pennsylvania; [§]Department of Chemistry, Institute for Biophysical Dynamics and the James Franck Institute, and [¶]Department of Physics, University of Chicago, Chicago, Illinois; [‖]Max Planck Institute of Colloids and Interfaces, Am Mühlenberg, Germany; and [††]Manuel Lujan Jr. Neutron Scattering Center, Los Alamos National Laboratory, Los Alamos, New Mexico

ABSTRACT The amphipathicity of the natively unstructured amyloid-β (Aβ40) peptide may play an important role in its aggregation into β-sheet rich fibrils, which is linked to the pathogenesis of Alzheimer's disease. Using the air/subphase interface as a model interface, we characterized Aβ's surface activity and its conformation, assembly, and morphology at the interface. Aβ readily adsorbed to the air/subphase interface to form a 20 Å thick film and showed a critical micelle concentration of ~120 nM. Aβ adsorbed at the air/subphase exhibited in-plane ordering that gave rise to Bragg peaks in grazing-incidence x-ray diffraction measurements. Analysis of the peaks showed that the air/subphase interface induced Aβ to fold into a β-sheet conformation and to self-assemble into ~100 Å-sized ordered clusters. The formation of these clusters at the air/subphase interface was not affected by pH, salts, or the presence of sucrose or urea, which are known to stabilize or denature native proteins, suggesting that interface-driven Aβ misfolding and assembly are strongly favored. Furthermore, Aβ at the interface seeded the growth of fibrils in the bulk with a distinct morphology compared to those formed by homogeneous nucleation. Our results indicate that interface-induced Aβ misfolding may serve as a heterogeneous, nucleation-controlled aggregation mechanism for Aβ fibrillogenesis in vivo.

INTRODUCTION

The amphipathic nature of the amyloid-β (Aβ) peptide, an endogenous 39–43 amino acid peptide whose misfolding and aggregation have been linked to the pathogenesis of Alzheimer's disease (AD), has been recognized for some time (1–5). To date, however, the driving forces and mechanism of Aβ aggregation in vivo remain unresolved. Aβ is derived from the proteolytic processing of the transmembrane amyloid-β precursor protein (APP) during regular cell metabolism. The C-terminus of Aβ belongs to the transmembrane domain of APP and is therefore hydrophobic, whereas the N-terminal region is located outside the cell membrane and is hydrophilic and charged. In vitro experiments have shown that the peptide is surface active, spontaneously adsorbing to the air/water interface, and exhibits classic surfactant-like behaviors such as micelle formation (3,5). Studies so far have been focused on Aβ micelles, which are formed at Aβ concentrations ranging from 17.5 (3) to 100 (6) μM, and have shown that these micelles can be on-pathway nuclei during Aβ fibrillogenesis (3,6). This type of Aβ micelle-mediated, homogeneous, nucleation-dependent polymerization explains the kinetics of Aβ fibril formation in vitro (3,6).

What remains unclear, however, is to what extent micelle-mediated fibrillogenesis reflects the pathway by which Aβ forms fibrils in vivo, since Aβ concentration in the cerebral spinal fluid is only subnanomolar (7). Because of the orders-of-magnitude discrepancy between in vivo Aβ concentration and Aβ critical micelle concentration (CMC) values reported to date, it is unlikely that micelle-mediated Aβ fibrillogenesis is the dominant in vivo pathway of Aβ aggregation.

The assembly of native Aβ into fibrils is accompanied by large and distinctive changes in the peptide's conformation. Under conditions that mimic the hydrophobic interior of the cell membrane, Aβ has a significant amount of α-helical structure (8). When assembled into fibrils, Aβ adopts the characteristic β-sheet structures found in amyloid fibrils (9). In physiological buffers at low Aβ concentrations, the peptide is largely a random, flexible chain (10) with some local structural motifs (11,12). Thus, regardless of the conformation adopted by native Aβ, the emergence of cytotoxic Aβ aggregates necessitates the formation of both intra- and intermolecular β-sheets. The lag phase that is observed during Aβ incubation in vitro before the appearance of fibrils reflects to a significant degree the energy barrier that must be overcome before the otherwise unfolded Aβ can adopt a β-sheet-rich conformation and oligomerize into ordered intermediates or protofibrils (13–15). One way to overcome this energy barrier is through the formation of Aβ micelles. However, for concentrations closer to the nanomolar in vivo condition, the driving force and molecular basis of the structural fluctuations of the native Aβ that misfold the peptide into the aggregation-competent β-sheet conformation remain poorly understood.

Aside from forming micelles in the bulk solution, the amphipathicity of Aβ also results in a peptide population

Submitted July 30, 2009, and accepted for publication January 20, 2010.

*Correspondence: kayeelee@uchicago.edu

Editor: Gerhard Hummer.

0006-3495/10/05/2299/10 $2.00

doi: 10.1016/j.bpj.2010.01.056

partitioned to an interface. It has been documented in many cases that interfaces can induce irreversible and nonnative aggregation of natively folded proteins (16,17). Aβ peptides are natively unstructured, and therefore it is not obvious that the adsorption of Aβ to an interface would impact its aggregation. However, there is increasing evidence that interfaces can modulate Aβ conformation and induce fibril formation, including solid surfaces (18) and liquid/liquid interfaces (19). The lipid membrane, which is a physiological interface, has been shown to accelerate Aβ fibrillogenesis (20–22). We have shown that Aβ favorably interacts with lipid membranes containing negatively charged lipids (2) and ganglioside G_{M1} (1). Furthermore, the membrane-associated Aβ readily seeds fibril growth, suggesting that membrane-induced Aβ fibrillogenesis may serve as a pathway for Aβ aggregation in vivo (1,23). The most striking result from our previous studies is that the association of the natively unfolded Aβ to the anionic membrane surface induces the formation of ordered assemblies that contain Aβ peptides folded in a β-sheet conformation (23,24). This finding provides a molecular basis for the observed membrane-induced Aβ aggregation and reveals a novel mechanism of protein aggregation, interface templated protein misfolding, and self-assembly. To better understand the generality of this mechanism, the dynamics of Aβ at interfaces with different chemical and physical characteristics also need to be investigated.

Here, we examine the effects of an idealized hydrophobic interface, the air/subphase interface, on the conformation, assembly state, and morphology of Aβ peptides at the interface. The air/subphase interface is known to perturb protein structure, where agitation is often used to accelerate protein aggregation. Additionally, the air/subphase interface may be responsible for generating structurally distinct Aβ fibril nuclei, seeding the growth of Aβ fibrils that are morphologically and structurally different from fibrils grown in quiescent samples (25). Thus, although the air/subphase interface is not a physiological one, it is important to study Aβ's interfacial dynamics at this interface to better understand Aβ's aggregation mechanism.

Previous studies reported that Aβ40 peptides at the air/subphase interface adopt a β-sheet conformation, and that β-sheets orient mostly parallel to the surface (4,26). Although these studies provided insights primarily into the secondary structure of the peptide, they gave little information about the higher-order supramolecular organization of Aβ at the interface. Here, we present the results of a multiscale characterization of the conformation and morphology of Aβ that spontaneously adsorbs to the air/subphase interface, and our investigation into whether these surface-adsorbed peptides can seed Aβ aggregation in the bulk solution. We used two surface-sensitive, complementary x-ray scattering techniques (grazing-incidence x-ray diffraction (GIXD) and x-ray reflectivity (XR)) to resolve in situ Å-level details, and atomic force microscopy (AFM) to resolve a submicron-level structure of Aβ adsorbed at the air/subphase interface. The effect of surface-adsorbed Aβ on its fibrillogenesis was further evaluated.

MATERIALS AND METHODS

Materials

Aβ40 peptide was synthesized, purified, and stored (1). The peptide was first dissolved in dimethyl sulfoxide (DMSO) to yield a 2 mg/mL (462 μM) stock solution. Phosphate-buffered saline (PBS; pH 7.4) was purchased from Invitrogen (Carlsbad, CA). Sucrose, urea, NaCl, NaH_2PO_4, Na_2HPO_4, and acetic acid were purchased from Fisher Scientific (Pittsburgh, PA). Thioflavin-T and sodium acetate (NaAc) were purchased from Sigma-Aldrich (St. Louis, MO). All water used was filtered through a Milli-Q Ultrapure water purification system (Millipore, Bedford, MA).

Aβ40 surface activity measurements

The surface activity of Aβ was evaluated by measuring the surface pressure (π) reached by the adsorption of Aβ to the air/subphase interface using a custom-made Langmuir trough (2). The Teflon trough consisted of two symmetric barriers, a Wilhelmy plate pressure sensor (Riegler and Kirstein, Berlin, Germany), and a resistively heated coverglass (Delta Technologies, Dallas, TX). All experiments were carried out at 30 $\pm$ 0.5°C.

First, the pressure sensor was calibrated, and the barriers were then compressed. An aliquot of 40 μM Aβ ranging from 50 to 1250 μL, diluted from the stock solution, was then injected into the 80 mL subphase of the trough. The Aβ concentration in the subphase thus ranged from 25 to 625 nM with 0.05–0.14 vol% DMSO present. Aβ was allowed to equilibrate and π was recorded. The final π reached by Aβ adsorption was taken as a measure of Aβ surface activity. The effects of subphase pH, salt, and cosolutes on π were also tested. The following subphase solutions were used: pH 5.5 10 mM NaAc with and without 140 mM NaCl, pH 6.5 10 mM sodium phosphate with and without 140 mM NaCl, pH 7.4 10 mM sodium phosphate with and without 140 mM NaCl, 0.25 and 1 M sucrose in water, and 2 and 6 M urea in water. A separate experiment was carried out for each Aβ concentration and subphase condition.

X-ray scattering experiments

GIXD and XR measurements on an Aβ film adsorbed at the air/subphase interface were carried out on the BW1 beamline at the HASYLAB synchrotron source (DESY, Hamburg, Germany) with a dedicated liquid surface diffractometer equipped with a Langmuir trough (27). All experiments were carried out at 30°C and at 250 nM Aβ subphase concentration. The Aβ film at the air/subphase interface was formed by equilibrium adsorption in the different subphase conditions described in the previous section.

Atomic force microscopy

To assess the morphology of the Aβ film adsorbed to the air/subphase interface, the peptide film was transferred from the Langmuir trough onto a mica substrate by inverse Langmuir-Shaefer transfer (28) and imaged by AFM. A freshly cleaved mica, mounted in a magnetic stainless-steel holder with a machined knife edge, was placed in the trough at the beginning of each experiment and remained submerged during the experiment. At the end of an experiment, the subphase was aspirated from the trough at a location outside of the barriers to lower the subphase level. As the subphase was lowered, the holder knife edge cut the Aβ film, resulting in its deposition on the mica. Aβ adsorbed to mica was also evaluated by placing a second mica in the subphase. At the end of an experiment, the mica was first moved, while submerged in the subphase, from inside the barriers to outside of the barriers. Then, the subphase was aspirated from above the second mica to remove any

surface-adsorbed Aβ and to lower the subphase level. Thus, the second mica contained only adsorbed Aβ. Mica pucks with transferred and/or adsorbed Aβ were imaged by AFM. To determine the thickness of the Aβ film transferred from the air/subphase interface, we adopted the tip scratching method (29). The peptide layer on the mica surface was scratched away by the AFM tip at 10 Hz and 4 V for 5 min; the mica was not damaged during the scratching. Several different scratches were measured for each film to allow statistical analysis of the data. The Aβ layer thickness was measured relative to the bare mica surface by line scan.

Incubation experiments

To investigate the effects of Aβ adsorbed at the air/subphase interface on fibrillogenesis, the peptide was incubated at 25°C either quiescently with a static air/subphase interface, continuously rotated end-to-end (about the long axis of the syringe) in one direction at 8 rpm (Barnstead/Thermolyne LabQuake Shaker Rotisserie) with an exposed air/subphase interface, or rotated with no air/subphase interface (overfilled). Aβ (25 μM) samples were prepared by diluting the Aβ stock solution and then incubating the samples in syringes (Norm Ject; Henke Sass Wolf Gmbh, Tuttlingen, Germany). Syringes were used because the air/subphase interface could be conveniently eliminated by adjusting the position of the plunger. Of importance, for the overfilled samples, the cylindrical geometry of the syringe barrel allowed bulk mixing to occur during rotation. Furthermore, the syringes were latex-free and did not have rubber septums (silicone oil, which is known to induce protein denaturation and aggregation (30), is often used as a lubricant for such septums). Aβ was incubated as individual aliquots to ensure that the samples were not disturbed before analysis.

At each time point, Aβ samples were taken for analysis. The fibrils were detected by Thioflavin-T (ThT) fluorescence and the morphology of Aβ fibrils were imaged by transmission electron microscopy (TEM; FEI Tecnai F30; FEI Co., Hillsboro, OR). Then 20 μL of Aβ sample were mixed with 2 mL of 10 μM ThT in PBS, and the fluorescence emission intensity of the sample ($\lambda_{Ex} = 446 \pm 3$ nm, $\lambda_{Em} = 490 \pm 10$ nm) was recorded (Flouromax-3; Horiva Jobin Yvon, Edison, NJ) (1). For TEM experiments, samples were applied to a glow-discharged, carbon-coated support film, washed, stained with 1% uranyl acetate, dried, and imaged.

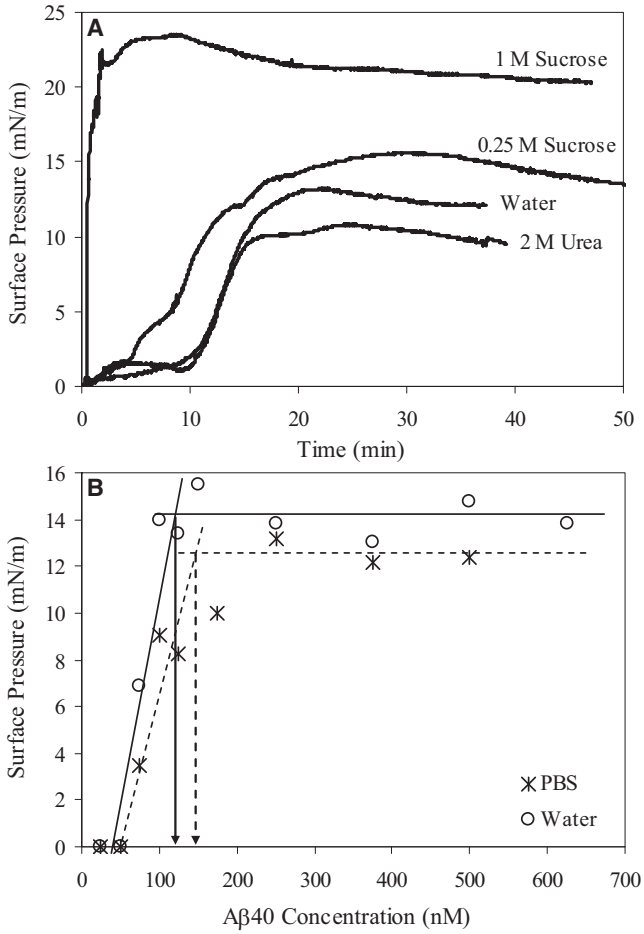

FIGURE 1 (*A*) Adsorption isotherms of Aβ in various subphase conditions. (*B*) Determination of the CMC values of Aβ in water (*circles* and *lines*) and PBS (*stars* and *dashed lines*). The extrapolated CMC values for Aβ in water and PBS were ~120 and 145 nM, respectively.

RESULTS

Surface activity of Aβ

The surface activity of Aβ40 was assessed by measuring the final π reached by the adsorption of Aβ from a bulk aqueous subphase to the air/subphase interface at 30°C (π is defined as the magnitude by which the surface tension of a pure air/subphase interface (σ_o) is reduced ($\pi = \sigma_o - \sigma$) by the presence of an adsorbate at the interface).

After Aβ was injected into the subphase of a Langmuir trough, the peptide spontaneously adsorbed to the air/subphase interface, resulting in a rise in π. The adsorption isotherm of Aβ on water in Fig. 1 *A* is representative of those measured on water and buffered subphases, where slow increases in π at short times were followed by a rapid rise in π, with π reaching a plateau at longer times. The average π-value reached for Aβ concentrations $>$ 250 nM was ~14 mN/m, which is in agreement with previously reported values (2,5,31). To determine the CMC of Aβ, π-values attained from different Aβ subphase concentrations were measured for water (Fig. 1 *B*, *open circles*) and pH 7.4 PBS (Fig. 1 *B*, *stars*). As shown, no rise in π was detected for Aβ concentrations $<$ 50 nM; π increased with increasing Aβ concentration beyond 50 nM and stayed constant for Aβ concentrations $>$ 200 nM. CMC values of Aβ in water and PBS, estimated from the intercepts of the two lines obtained from fitting π-values versus concentration above and below the CMC, were roughly 120 and 145 nM, respectively (Fig. 1 *B*). Aβ thus exhibits significant surface activity in the low (nanomolar) concentration regime. Note that these CMC values are ~2–3 orders of magnitude smaller than some previously reported values (3,5,6), but the discrepancies can be accounted for by the different experimental conditions (e.g., Aβ concentrations, pH, temperature, and solvent) and methodologies employed. In this study, we focused on Aβ surface activity in a low (nanomolar) concentration regime in an effort to study the peptide's behavior at concentrations closer to those found in vivo, and extrapolated our CMC values directly from surface tension measurements, rather than from, e.g., kinetics data (6). Low CMC values have previously been reported with experimental protocols similar to ours (31).

To assess the effects of neutral cosolutes on the surface activity of Aβ, we tested the adsorption of Aβ to the air/subphase interface in the presence of a protein-stabilizing cosolute sucrose and a protein-denaturing cosolute urea. Sucrose is known to nonspecifically stabilize globular proteins against denaturation and aggregation in solution by driving the protein native-state ensemble toward more compact conformations (32,33). In contrast, urea is a chaotrope that solubilizes and unfolds proteins (34). As shown in Fig. 1 *A*, the cosolutes affected both the rate of Aβ adsorption and the final π reached. In water containing 1 M sucrose, π increased immediately upon Aβ injection. Aβ adsorption occurred at a much faster rate and achieved a significantly higher π compared to adsorption from water. In water containing 2 M urea, the Aβ adsorption rate was similar to that in water, except that a lower final π was achieved.

Structure of Aβ at the air/subphase interface measured by GIXD and XR

Complementary surface-sensitive GIXD and XR measurements were made to investigate in situ the molecular structure of the Aβ film at the air/subphase interface. GIXD measurements provide structural information on the in-plane ordered (diffracting) portion of the film, whereas XR measurements provide information on the laterally averaged electron density distribution (ρ) perpendicular to the interface (27,35). By combining the two techniques, we were able to achieve the first structural characterization (to our knowledge) of Aβ adsorbed at the air/subphase interface with Å resolution.

GIXD data of Aβ adsorbed to the air/subphase interface at all pH, salt, and cosolute subphase conditions tested showed a Bragg peak at $q_{xy} = 1.32$ Å^{-1} (Fig. 2). The presence of the Bragg peak indicated the existence of an ordered structure in the adsorbed Aβ film. Each background-subtracted peak could be fit with a single Gaussian function and is indicative of one characteristic d-spacing. The q_{xy}-values of the maxima and the full width at half-maximum of the Bragg peaks were used to calculate the d-spacing ($d = 2\pi/q_{xy}$) and coherence length (the distance over which the in-plane order extends, L_c) of the ordered Aβ structure, respectively (Table 1). In water and buffers, the Bragg peaks corresponded to a d-spacing value of 4.75 Å (Table 1). At the low Aβ concentration of 250 nM used in our experiments, fibril formation was not expected; surprisingly, the d-spacing exactly matched the β-sheet spacing between Aβ monomers found by diffraction of amyloid fibers (25,36). L_c values associated with the Bragg peaks obtained in water or buffer were ~100 Å (Table 1). Thus, the diffracting crystallites were comprised of ~20 Aβ peptides assembled in a β-sheet conformation. In this conformation, the β-sheets are likely oriented parallel to the air/subphase interface, as earlier studies using infrared reflection absorption spectroscopy have shown (37). Although the exact shape of the Aβ

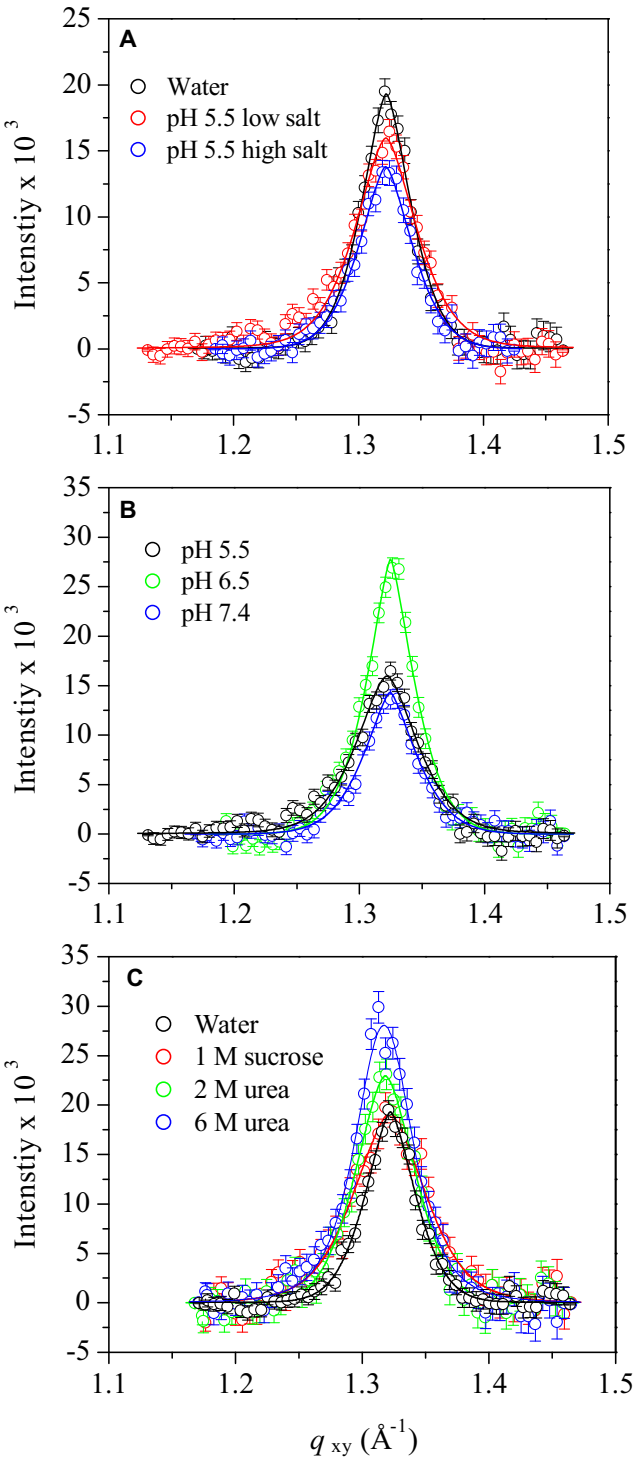

FIGURE 2 Background-subtracted Bragg peak profiles from GIXD data of Aβ adsorbed to the air/subphase interface at 30°C. (*A*) Effect of ionic strength on the Bragg peak profile of Aβ at pH 5.5. Low-salt buffer contained 10 mM sodium acetate, and high-salt buffer contained 10 mM sodium acetate and 140 mM NaCl. (*B*) Effect of pH on the Bragg peak profiles of Aβ in 10 mM salt buffers. (*C*) Effect of neutral cosolutes on the Bragg peak profiles of Aβ in water. Solid lines are fits to the data.

TABLE 1 Parameters obtained from GIXD data of Aβ films at the air/subphase interface at 30°C

Subphase condition	d -spacing (Å)	Coherence length L_c (Å)
Water	4.752	123.6
pH 5.5 10 mM sodium citrate	4.753	98.06
pH 5.5 10 mM sodium citrate, 140 mM sodium chloride	4.748 ± 0.008*	111.3 ± 9.3*
pH 6.5 10 mM sodium phosphate	4.748	129.5
pH 6.5 10 mM sodium citrate, 140 mM sodium chloride	4.746	108.8
pH 7.4 10 mM sodium phosphate	4.744	116.7
pH 7.4 PBS	4.741 ± 0.002*	109.9 ± 15*
1 M sucrose in water	4.755	85.52
2 M urea in water	4.766	102.8
6 M urea in water	4.770	105.4

*Average and standard deviation (SD) values of fitted parameters obtained from multiple experiments.

clusters or the registry of the β-sheets (i.e., parallel or anti-parallel) cannot be extrapolated from the data presented here, they may constitute Aβ oligomers or protofibrils at an interface.

XR data of Aβ adsorbed to the air/subphase interface were fit and modeled using the *StochFit* fitting routine (38), which first provided a stochastic model-independent ρ fit of the reflectivity data, after which ρ was fit to a box model with smeared interfaces to extract physically meaningful results. A one-box model with one roughness value at the air/Aβ interface ($\sigma_{air/A\beta}$) and another roughness value at the Aβ/subphase interface ($\sigma_{A\beta/subphase}$) provided excellent fits to the model-independent ρ of each Aβ film (not shown). Fig. 3 *A* shows select normalized reflectivity data ($R/R_{F,subphase}$) and their corresponding model-independent ρ fits (Fig. 3, *B* and *C, solid curves*) and the one-box model-dependent fits (Fig. 3, *B* and *C*, dashed lines). Fitting parameters are summarized in Table 2.

As shown in Fig. 3 *A*, $R/R_{F,subphase}$ of Aβ films adsorbed from water (*black*) and a buffer subphase (pH 6.5, 10 mM sodium phosphate and 140 mM NaCl, *red*) overlapped; in fact, $R/R_{F,subphase}$ of Aβ adsorbed from water and buffer subphases in the pH range (pH 5.5–7.4) and ionic strength conditions (0–150 mM salt concentration) tested all showed good overlap (data not shown). Fitting of the XR data yielded films with thicknesses of ~20 Å (Table 2), with a $\sigma_{air/A\beta}$ value of ~2.7 Å, which is close to the 3 Å expected from the thermally excited capillary waves, and a $\sigma_{A\beta/subphase}$ value of ~7.8 Å. This larger $\sigma_{A\beta/subphase}$ value indicates that a portion of Aβ, likely the unstructured hydrophilic N-terminus, is extended into the subphase, creating a more smeared interface. In the presence of 1 M sucrose, the Aβ film thickness and ρ/ρ_{water} did not change. However, $\sigma_{A\beta/subphase}$ decreased to 5.0 Å (Table 2). This decrease is likely due to the preferential exclusion of sucrose at the Aβ/subphase interface, where a more compact conformation

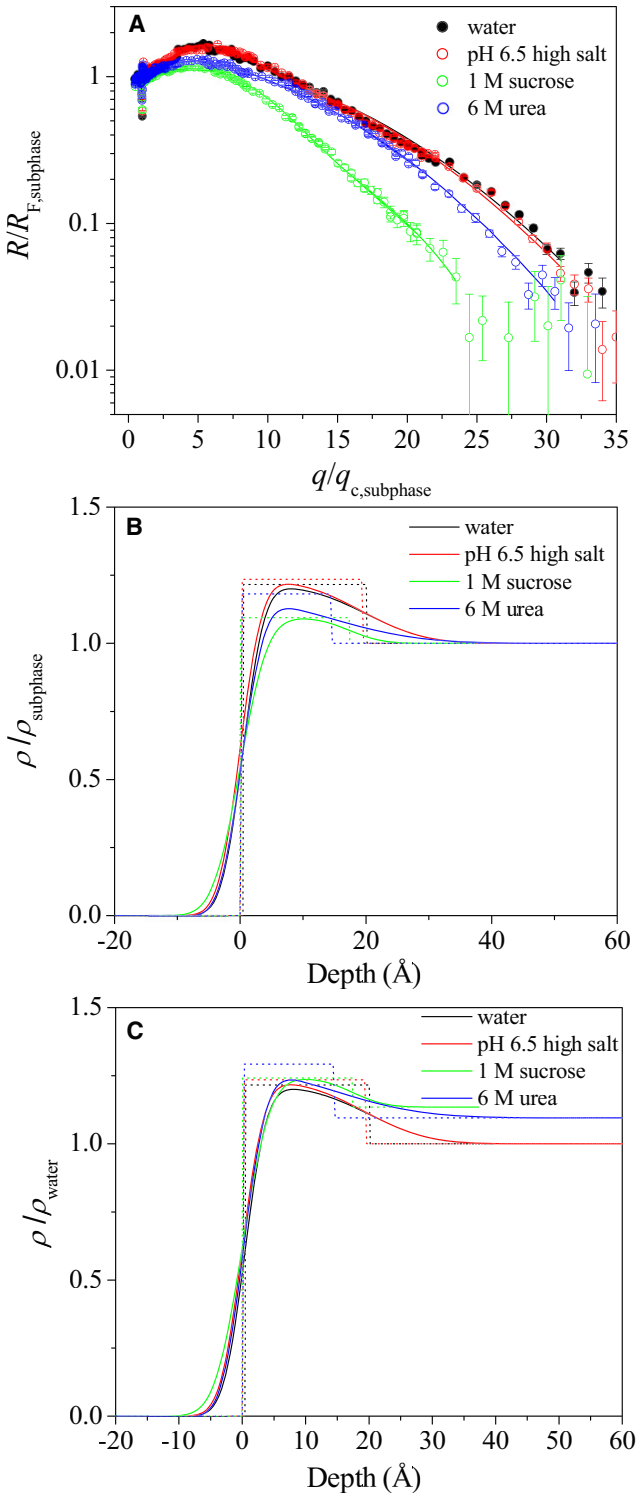

FIGURE 3 (*A*) Open symbols show the Fresnel normalized reflectivity data (R/R_F) and fits for Aβ adsorbed to the air/subphase interface at 30°C. The solid lines represent the model-dependent fit to the reflectivity curves obtained from *StochFit* fitting routine. A one-box model with two roughness parameters was used to fit all of the reflectivity data (*dashed lines*). Corresponding electron density profiles of Aβ adsorbed at the air/subphase interface (*B*) normalized to $\rho_{subphase}$ and (*C*) normalized to ρ_{water} are shown. Both smeared (*solid line*) and unsmeared (*dotted line*) electron density profiles are plotted. Negative depth values denote air, and positive depth values denote the subphase.

TABLE 2 Fitting parameters from XR data Aβ adsorbed at the air/subphase interface at 30°C

Subphase condition	Thickness L_z (Å)	Normalized electron density		Interfacial roughness σ (Å)	
		$\rho/\rho_{subphase}$	ρ/ρ_{water}	$\sigma_{air/A\beta}$	$\sigma_{A\beta/subphase}$
Water	19.9 ± 0.014	1.21 ± 0.21	1.21 ± 0.21	2.65 ± 0.003	7.48 ± 0.22
pH 6.5 10mM sodium phosphate, 140mM sodium chloride	19.4 ± 0.009	1.24 ± 0.14	1.24 ± 0.14	2.74 ± 0.002	7.73 ± 0.14
pH 7.4 PBS	20.4 ± 0.009	1.23 ± 0.14	1.23 ± 0.14	2.92 ± 0.002	8.15 ± 0.14
1M sucrose in water	19.2 ± 0.006	1.10 ± 0.093	1.24 ± 0.011	3.42 ± 0.0008	5.04 ± 0.011
2M urea in water	13.1 ± 0.008	1.30 ± 0.27	1.34 ± 0.28	3.37 ± 0.0057	11.1 ± 0.14
6M urea in water	14.2 ± 0.005	1.18 ± 0.26	1.294 ± 0.28	2.81 ± 0.0031	11.1 ± 0.15

Errors reported are SDs obtained from the nonlinear least-square fitting of the reflectivity data with a one-box model using the Levenberg-Marquardt algorithm (38).

of the unstructured Aβ N-terminus is favored. In the presence of the denaturing urea, the Aβ film thickness was smaller (14 Å) and $\sigma_{A\beta/subphase}$ values were larger (11 Å; Table 2). Taken together, these differences suggest that urea solubilized the non-β-sheet portion of Aβ, and that the peptide extended further into the subphase.

Morphology of Aβ at the air/water interface imaged by AFM

The submicron-level morphology of Aβ adsorbed at the air/subphase interface was assessed by transferring the Aβ film onto mica and then imaging the film by AFM. As shown in Fig. 4, Aβ adsorbed at the air/water interface for 2 h showed a uniform morphology (Fig. 4, *A1* and *A2*) composed of small round bumps that are brighter in the AFM images. The morphology of the film did not change over time, as the AFM image of an Aβ film transferred from the air/water interface after incubation in the Langmuir trough for 19 h showed very similar features (data not shown). The height and width of the bumps were ~20 and 200 Å, respectively. The width may be an overestimation of the actual size of these features since the lateral resolution was limited by the size of the AFM tip (~100 Å radius). In contrast to Aβ adsorbed at the air/water interface, Aβ at an air/PBS interface was much smoother and had few distinguishing features except for a few higher bright spots (Fig. 4, *B1* and *B2*), which were likely salt crystals from the buffer.

Because Aβ could also adsorb to mica from the bulk subphase, care was taken to assess the extent of Aβ adsorption and the morphology of the adsorbed Aβ. A representative AFM image of Aβ in water adsorbed on mica is shown in Fig. 4 *A3*. Clearly, Aβ adsorbed to the mica surface. However, the adsorbed Aβ film had much less roughness than the transferred film (Fig. 4 *A2*). The features in Fig. 4, *A1* and *A2*, are thus those of the Aβ film transferred from the air/water interface, and not an artifact of Aβ adsorption. In contrast, Aβ did not adsorb to the mica surface from a PBS subphase, likely due to the repulsive electrostatic interaction between Aβ (−3 charge) and the weakly negatively charged mica in PBS. In water at pH 5.5, Aβ is overall neutral and its positively charged residues can favorably interact with mica.

The thicknesses of the Aβ films were determined by means of the AFM tip scratching method (29). The thickness of the transferred and adsorbed Aβ layer (Fig. 4 *A1*), relative to the bare mica surface, was 40.1 ± 2.4 Å, and that of the

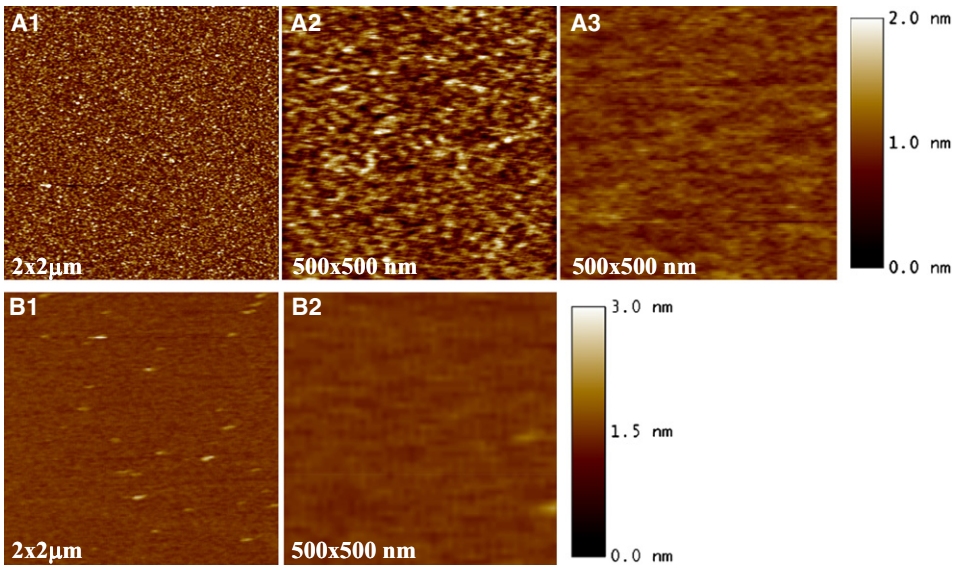

FIGURE 4 AFM images of Aβ transferred from the (*A1* and *A2*) air/water and (*B1*and *B2*) air/PBS interfaces. (*A3*) Aβ adsorbed to a mica surface from the bulk was also imaged.

adsorbed Aβ layer (Fig. 4 *A3*) was 23.1 $\pm$ 2.2 Å. Thus, assuming that the adsorbed and the transferred Aβ layers lie on top of one another without significant structural rearrangements, the thickness of Aβ transferred from the air/water interface is roughly the difference between the two samples, or 17.9 $\pm$ 3.3 Å, which is in good agreement with XR data. The thickness of the Aβ layer transferred from the air/PBS subphase (Fig. 4 *B1*) was 22.4 $\pm$ 2.6 Å. Similar to the case with PBS, the thickness of the Aβ film transferred from a pH 7.4 buffer (10 mM sodium phosphate) was 21.5 $\pm$ 0.3 Å. Taking all of the data into account, the thickness values of the transferred film obtained from AFM measurements are in general agreement with L_z values obtained from XR measurements (Table 2).

Effect of air/subphase interface-adsorbed Aβ on fibril formation

To investigate the role of surface-adsorbed Aβ on its fibrillogenesis in solution, Aβ samples were incubated such that the surface-adsorbed Aβ was reintroduced into the bulk and its effect on fibril formation was monitored. To achieve this, the Aβ solution with an exposed air/subphase interface was rotated. Since rotation also introduces mixing, which can increase aggregation kinetics and fragment aggregates, Aβ samples were also incubated in an overfilled configuration with no air/subphase interface. These rotated, overfilled samples captured the effects of mixing but eliminated the possible influence of the air/subphase interface, thus allowing us to isolate the effect of surface-adsorbed Aβ on fibrillogenesis. As controls, Aβ samples with an exposed air/subphase interface were also quiescently incubated, allowing us to monitor homogeneous nucleation and polymerization of Aβ under the same solution conditions.

Aβ samples were incubated either quiescently or rotated in pH 5.5 10 mM sodium acetate with and without NaCl, pH 6.5 10 mM sodium phosphate with and without NaCl, or pH 7.4 10 mM sodium phosphate with and without NaCl. At 25 μM Aβ, no increases in ThT fluorescence signal were observed for quiescently incubated samples at pH 5.5 and 6.5 for >30 days. However, large increases in ThT fluorescence were observed for pH 7.4 samples after 5 days of lag time. Fig. 5 *A1* shows a TEM image of a sample quiescently incubated for 36 days that formed aggregates at pH 7.4 (10 mM sodium phosphate). It can be seen that long individual Aβ fibrils with characteristic twists (*arrows* in Fig. 5 *A1*) were formed. In contrast, rotated Aβ samples in all buffers showed increases in ThT fluorescence with incubation time (data not shown). TEM images of Aβ samples rotated for 12 days show short and laterally associated fibrils that are straight and largely devoid of resolvable twists (Fig. 5, *A2–A4*). Increasing the ionic strength by adding

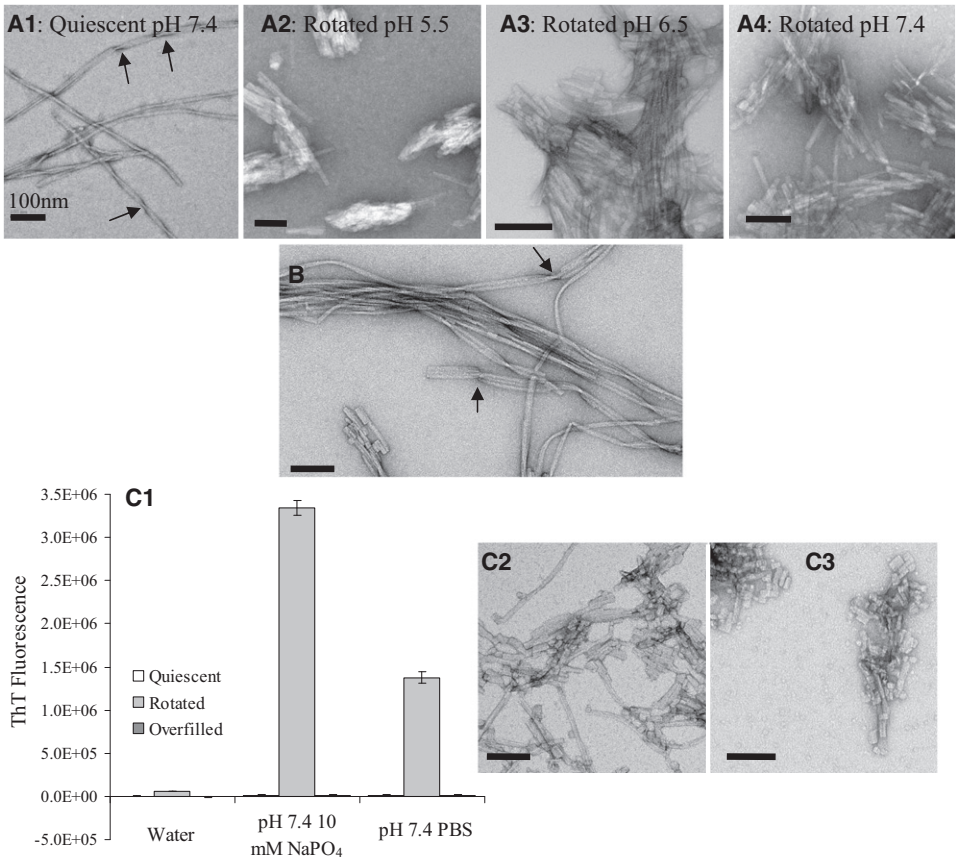

FIGURE 5 TEM images of 25 μM Aβ fibrils obtained in various solution conditions using different incubation methods: (*A1*) Aβ quiescently incubated in pH 7.4 10 mM sodium phosphate buffer for 36 days, (*A2*) Aβ rotated in pH 5.5 10 mM sodium acetate buffer for 12 days, (*A3*) Aβ rotated in pH 6.5 10 mM sodium phosphate buffer for 12 days, (*A4*) Aβ rotated in pH 7.4 10 mM sodium phosphate buffer for 12 days, and (*B*) Aβ rotated in PBS for 1 day and quiescently incubated for 5 days. (*C1*) Background-subtracted ThT fluorescence of Aβ in different solution conditions (pure water, pH 7.4 10 mM sodium phosphate buffer, and pH 7.4 PBS) and incubated using different incubation methods. ThT signals of quiescently incubated samples are plotted to the left of the rotated samples, and overfilled samples are plotted to the right of the rotated samples. TEM images of the fibrils formed in the (*C2*) Aβ samples rotated in pH 7.4 10 mM sodium phosphate and (*C3*) pH 7.4 PBS are shown.

NaCl did not affect the ThT signals measured for quiescently incubated or rotated samples for all three pH conditions tested.

A TEM image of an Aβ sample in pH 7.4 PBS that was rotated for 1 day and then quiescently incubated for 5 days is shown in Fig. 5 *B*. The aggregates show fibrils of mixed morphologies, i.e., both long and short fibrils, laterally associated fibrils, and laterally associated fibrils with twists (*arrows* in Fig. 5 *B*).

To isolate the two effects of sample rotation, remixing of air/subphase interface-adsorbed Aβ into the bulk, and mixing of the bulk solution, we collected ThT signal and TEM images of quiescent, rotated, and rotated overfilled samples. After 11 days, the quiescent samples did not show any increases in ThT signal or detectable aggregates in water or in pH 7.4 buffer solutions (Fig. 5 *C1*). The rotated sample in water showed a small increase in ThT signal and a few largely amorphous aggregates (image not shown), whereas the rotated samples in the two pH 7.4 buffers showed large increases in ThT and short, laterally associated, and straight fibrils (Fig. 5, *C2* and *C3*). The rotated overfilled samples, in contrast, did not give rise to increases in ThT fluorescence and showed no detectable aggregates in TEM images under all three conditions.

DISCUSSION

The mechanism and driving forces of in vivo Aβ aggregation linked to the pathogenesis of AD are still unclear. In vitro, the natively unstructured Aβ40 peptide displays a remarkable ability to form ordered fibrillar aggregates of different molecular-level structures (39–41). The fibril structure is not uniquely determined by the amino acid sequence of the constituent Aβ monomers; rather, it depends on experimental conditions. A recent study showed that Aβ40 fibrils seeded from fibrils extracted from brain tissues of deceased AD patients differed from the structures of purely synthetic Aβ40 fibrils (41). It has been hypothesized that the observed variations in fibril morphology and molecular structure arise from the existence of multiple, distinct fibril nucleation events (25). To gain an understanding of the molecular origin of different nucleation events, we investigated the interfacial dynamics of Aβ40 and its role in the peptide's fibrillogenesis.

Our study shows that the amphipathic Aβ40 (Fig. 6 *A*) is highly surface-active and spontaneously adsorbs to the air/subphase interface to form a contiguous, single-molecule (~20 Å thick) film. Moreover, the film contains ~100 Å-sized ordered domains comprised of Aβ peptides folded in a β-sheet conformation. Thus, when the otherwise unfolded Aβ partitions to the interface, the peptide misfolds into a conformation found in amyloid fibrils, and this conformation propagates ~20 peptides. This interface-driven misfolding and self-assembly of Aβ is observed at nanomolar peptide concentrations, far below the concentration at which Aβ

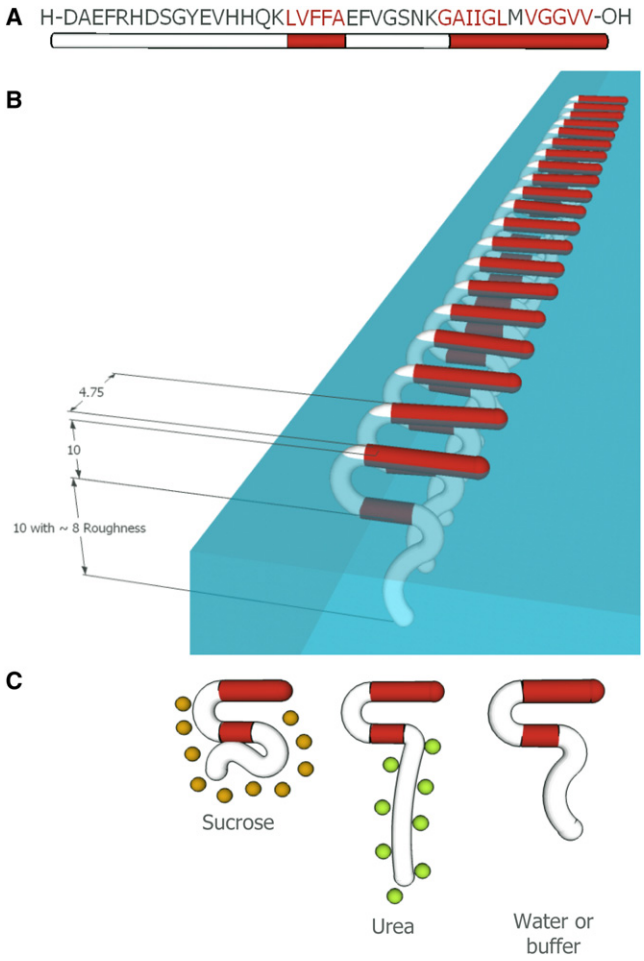

FIGURE 6 (*A*) Amino acid sequence of the Aβ40 peptide. Hydrophobic residues are shown in red. (*B*) Schematic of a crystalline domain of Aβ adsorbed at the air/subphase interface, reflecting the in-plane ordering from GIXD data and out-of-plane thickness and roughness values from XR data. The β-sheets depicted here are in registry (based on previous NMR studies (25,36,42)) and oriented parallel to the air/subphase interface (based on earlier studies using infrared reflection absorption spectroscopy (37)). (*C*) Effects of the neutral cosolutes sucrose (*orange circles*) and urea (*green circles*) on Aβ adsorbed to the air/subphase interface. The preferentially excluded sucrose decreases the roughness of the peptide/subphase interface, and the preferentially bound urea solvates the hydrophilic Aβ N-terminus, increasing the roughness of the peptide/subphase interface. All numbers are in Angstroms.

aggregation occurs in the bulk solution by homogeneous nucleation. Furthermore, the formation of ordered oligomers is not affected by pH (5.5–7.4) or ionic strength (0–150 mM salt), since ordered oligomers were formed under all conditions tested. The pH influences the charge and charge distribution on proteins, and can affect both their conformational stability and colloidal stability (e.g., protein-protein interactions) (32). The ionic strength mediates electrostatic interactions. Since Aβ is intrinsically unstructured, the effect of charge on conformational stability is expected to be weak. However, the charge effect on protein-protein interactions, and hence their association, is expected to be strong.

Protein-protein interactions affect assembly processes in solution, including homogeneous nucleation and fibril growth. The lack of an effect of pH and ionic strength on the formation of assembled Aβ clusters at the air/subphase interface indicates that the misfolding and association of Aβ at the air/subphase interface is primarily hydrophobicity driven. Moreover, these ordered oligomers are observed even in the presence of 6 M urea, indicating that the driving force for Aβ misfolding and assembly at the air/subphase interface is strong.

Fig. 6 *B* shows a schematic of an ordered Aβ oligomer at the air/subphase interface, reflecting the in-plane ordering and out-of-plane thickness and roughness values obtained from x-ray scattering experiments. The orientation of the β-sheets is depicted as being parallel to the air/subphase interface, based on earlier studies using infrared reflection absorption spectroscopy (37). Although we cannot distinguish whether the peptides are assembled in the parallel or antiparallel β-sheet configuration, solid-state NMR studies have shown that the cross-β motif in Aβ40 fibrils is composed of in-register, parallel β-sheets (25,36,42). Hence, the parallel case is depicted here. Moreover, our study shows that the presence of neutral cosolutes (sucrose or urea) at concentrations known to stabilize or denature native protein structures in solution does not enhance or prevent the formation of the ordered oligomers at an interface. The cosolutes, however, do affect the structure of the peptide at the air/subphase interface (Fig. 6 *C*). The preferentially excluded sucrose decreases the roughness value of the peptide/subphase interface, and the preferentially bound urea solvates the hydrophilic Aβ N-terminus, increasing the roughness of the peptide/subphase interface. Moreover, sucrose greatly enhances the surface activity of Aβ, with the peptide adsorbing to the air/subphase interface at a much faster rate and attaining a significantly higher surface pressure in the presence of 1 M sucrose (Fig. 1 *A*). The cellular environment is known to be molecularly crowded, and the concentration of macromolecules and cosolutes can be as high as 350 mg/mL (43). Thus, the surface activity of Aβ observed under the dilute solution conditions used in this study may be much more pronounced in the cellular environment.

The incubation results obtained in this study show that interface-adsorbed Aβ can seed fibril formation when it is reintroduced into the bulk. Eliminating the interface effectively inhibits fibril formation. Moreover, fibrils formed by seeding with interface-adsorbed Aβ show different morphological characteristics compared to those formed by homogeneous nucleation after long incubation times. Seeded fibrils tend to be straight and laterally associated, whereas unseeded fibrils are predominantly individual fibrils with periodic twists (25,39,41,44). Our study offers an explanation of the molecular origin of the observed fibril polymorphism: ordered oligomers formed at the air/subphase interface represent a distinct nucleus for Aβ fibril growth.

The interfacial dynamics of the Aβ peptide thus plays an important role in its aggregation into amyloid fibrils, and may constitute a driving force for in vivo Aβ aggregation at low physiological concentrations. Our results indicate that interface-induced Aβ folding and self-assembly may serve as a heterogeneous nucleation-controlled aggregation mechanism whereby Aβ aggregates in vivo.

We thank H. Miller-Auer and S. Meredith for their help with peptide synthesis, and Y. Chen for her help with fibril imaging. We thank the staff of HASYLAB (DESY, Hamburg, Germany) for providing beamtime on the BW1 beamline. We acknowledge the Biophysical Core Facility (University of Chicago) for the use of the Flouromax-3 spectrofluorometer.

The Langmuir trough was made possible by a National Science Foundation (NSF) Chemistry Research Instrumentation and Facilities Program Junior Faculty Grant (CHE-9816513). This work was supported by the Alzheimer's Association (IIRG-9901175), the American Health Assistance Foundation (A1999057), the Packard Foundation, the U.S. Department of Energy (W-7405-ENG-36), and the NSF Materials Research and Engineering Centers Programs (DMR-0820054). E.Y.C. received a National Institutes of Health National Research Service Award Individual Fellowship (AG025649). S.L.F. received support from the NSF Graduate Fellowship Program. A.W. was a Beckman Scholar and received support from the Arnold and Mabel Beckman Foundation. Travel was supported by a I2CAM Junior Scientists Travel Award.

REFERENCES

1. Chi, E. Y., S. L. Frey, and K. Y. C. Lee. 2007. Ganglioside G(M1)-mediated amyloid-β fibrillogenesis and membrane disruption. *Biochemistry*. 46:1913–1924.
2. Ege, C., and K. Y. C. Lee. 2004. Insertion of Alzheimer's Aβ40 peptide into lipid monolayers. *Biophys. J.* 87:1732–1740.
3. Sabaté, R., and J. Estelrich. 2005. Evidence of the existence of micelles in the fibrillogenesis of β-amyloid peptide. *J. Phys. Chem. B.* 109:11027–11032.
4. Schladitz, C., E. P. Vieira, …, H. Möhwald. 1999. Amyloid-β-sheet formation at the air-water interface. *Biophys. J.* 77:3305–3310.
5. Soreghan, B., J. Kosmoski, and C. Glabe. 1994. Surfactant properties of Alzheimer's Aβ peptides and the mechanism of amyloid aggregation. *J. Biol. Chem.* 269:28551–28554.
6. Lomakin, A., D. S. Chung, …, D. B. Teplow. 1996. On the nucleation and growth of amyloid β-protein fibrils: detection of nuclei and quantitation of rate constants. *Proc. Natl. Acad. Sci. USA.* 93:1125–1129.
7. Seubert, P., C. Vigo-Pelfrey, …, D. Schenk. 1992. Isolation and quantification of soluble Alzheimer's β-peptide from biological fluids. *Nature.* 359:325–327.
8. Barrow, C. J., and M. G. Zagorski. 1991. Solution structures of β peptide and its constituent fragments: relation to amyloid deposition. *Science.* 253:179–182.
9. Sunde, M., and C. Blake. 1997. The structure of amyloid fibrils by electron microscopy and X-ray diffraction. *Adv. Protein Chem.* 50: 123–159.
10. Barrow, C. J., A. Yasuda, …, M. G. Zagorski. 1992. Solution conformations and aggregational properties of synthetic amyloid β-peptides of Alzheimer's disease. Analysis of circular dichroism spectra. *J. Mol. Biol.* 225:1075–1093.
11. Hou, L. M., H. Y. Shao, …, M. G. Zagorski. 2004. Solution NMR studies of the Aβ (1-40) and Aβ (1-42) peptides establish that the Met35 oxidation state affects the mechanism of amyloid formation. *J. Am. Chem. Soc.* 126:1992–2005.
12. Sgourakis, N. G., Y. L. Yan, …, A. E. Garcia. 2007. The Alzheimer's peptides Aβ40 and 42 adopt distinct conformations in water: a combined MD/NMR study. *J. Mol. Biol.* 368:1448–1457.

13. Esler, W. P., A. M. Felix, …, J. E. Maggio. 2000. Activation barriers to structural transition determine deposition rates of Alzheimer's disease Aβ amyloid. *J. Struct. Biol.* 130:174–183.

14. Fezoui, Y., and D. B. Teplow. 2002. Kinetic studies of amyloid β-protein fibril assembly. Differential effects of α-helix stabilization. *J. Biol. Chem.* 277:36948–36954.

15. Sciarretta, K. L., D. J. Gordon, …, S. C. Meredith. 2005. Aβ40-Lactam(D23/K28) models a conformation highly favorable for nucleation of amyloid. *Biochemistry.* 44:6003–6014.

16. Sethuraman, A., and G. Belfort. 2005. Protein structural perturbation and aggregation on homogeneous surfaces. *Biophys. J.* 88:1322–1333.

17. Chi, E. Y., J. Weickmann, …, T. W. Randolph. 2005. Heterogeneous nucleation-controlled particulate formation of recombinant human platelet-activating factor acetylhydrolase in pharmaceutical formulation. *J. Pharm. Sci.* 94:256–274.

18. Kowalewski, T., and D. M. Holtzman. 1999. In situ atomic force microscopy study of Alzheimer's β-amyloid peptide on different substrates: new insights into mechanism of β-sheet formation. *Proc. Natl. Acad. Sci. USA.* 96:3688–3693.

19. Nichols, M. R., M. A. Moss, …, T. L. Rosenberry. 2005. Amyloid-β aggregates formed at polar-nonpolar interfaces differ from amyloid-β protofibrils produced in aqueous buffers. *Microsc. Res. Tech.* 67: 164–174.

20. Yip, C. M., E. A. Elton, …, J. McLaurin. 2001. Cholesterol, a modulator of membrane-associated Aβ-fibrillogenesis and neurotoxicity. *J. Mol. Biol.* 311:723–734.

21. McLaurin, J., and A. Chakrabartty. 1997. Characterization of the interactions of Alzheimer β-amyloid peptides with phospholipid membranes. *Eur. J. Biochem.* 245:355–363.

22. Terzi, E., G. Hölzemann, and J. Seelig. 1997. Interaction of Alzheimer β-amyloid peptide(1-40) with lipid membranes. *Biochemistry.* 36:14845–14852.

23. Chi, E. Y., C. Ege, …, K. Y. Lee. 2008. Lipid membrane templates the ordering and induces the fibrillogenesis of Alzheimer's disease amyloid-β peptide. *Proteins.* 72:1–24.

24. Ege, C., J. Majewski, …, K. Y. Lee. 2005. Templating effect of lipid membranes on Alzheimer's amyloid β peptide. *ChemPhysChem.* 6:226–229.

25. Tycko, R. 2006. Molecular structure of amyloid fibrils: insights from solid-state NMR. *Q. Rev. Biophys.* 39:1–55.

26. Brezesinski, G., E. Maltseva, and H. Mohwald. 2007. Adsorption of amyloid-β (1–40) peptide at liquid interfaces. *Z. Phys. Chem.* 221: 95–111.

27. Jensen, T. R., and K. Kjaer. 2001. Structural properties and interactions of thin films at the air-liquid interface explored by synchrotron x-ray scattering. *In* Novel Methods to Study Interfacial Layers. D. Mobius and R. Miller, editors. Elsevier Science, Amsterdam. 205–254.

28. Lee, K. Y. C., M. M. Lipp, …, A. J. Waring. 1998. Apparatus for the continuous monitoring of surface morphology via fluorescence microscopy during monolayer transfer to substrates. *Langmuir.* 14:2567–2572.

29. Heyman, A., I. Medalsy, …, O. Shoseyov. 2009. Float and compress: honeycomb-like array of a highly stable protein scaffold. *Langmuir.* 25:5226–5229.

30. Jones, L. S., A. Kaufmann, and C. R. Middaugh. 2005. Silicone oil induced aggregation of proteins. *J. Pharm. Sci.* 94:918–927.

31. Ji, S. R., Y. Wu, and S. F. Sui. 2002. Study of β-amyloid peptide (Aβ40) insertion into phospholipid membranes using monolayer technique. *Biochemistry (Mosc.).* 67:1283–1288.

32. Chi, E. Y., S. Krishnan, …, T. W. Randolph. 2003. Roles of conformational stability and colloidal stability in the aggregation of recombinant human granulocyte colony-stimulating factor. *Protein Sci.* 12:903–913.

33. Timasheff, S. N. 1998. Control of protein stability and reactions by weakly interacting cosolvents: the simplicity of the complicated. *Adv. Protein Chem.* 51:355–432.

34. Pace, C. N. 1986. Determination and analysis of urea and guanidine hydrochloride denaturation curves. *Methods Enzymol.* 131:266–280.

35. Als-Nielsen, J., D. Jacquemain, …, L. Leiserowitz. 1994. Principles and applications of grazing incidence X-ray and neutron scattering from ordered molecular monolayers at the air-water interface. *Phys. Rep.* 246:251–313.

36. Benzinger, T. L., D. M. Gregory, …, S. C. Meredith. 2000. Two-dimensional structure of β-amyloid(10-35) fibrils. *Biochemistry.* 39: 3491–3499.

37. Maltseva, E., A. Kerth, …, G. Brezesinski. 2005. Adsorption of amyloid β (1-40) peptide at phospholipid monolayers. *ChemBioChem.* 6:1817–1824.

38. Danauskas, S. M., D. X. Li, …, K. Y. C. Lee. 2008. Stochastic fitting of specular X-ray reflectivity data using StochFit. *J. Appl. Cryst.* 41: 1187–1193.

39. Petkova, A. T., R. D. Leapman, …, R. Tycko. 2005. Self-propagating, molecular-level polymorphism in Alzheimer's β-amyloid fibrils. *Science.* 307:262–265.

40. Wetzel, R., S. Shivaprasad, and A. D. Williams. 2007. Plasticity of amyloid fibrils. *Biochemistry.* 46:1–10.

41. Paravastu, A. K., I. Qahwash, …, R. Tycko. 2009. Seeded growth of β-amyloid fibrils from Alzheimer's brain-derived fibrils produces a distinct fibril structure. *Proc. Natl. Acad. Sci. USA.* 106:7443–7448.

42. Petkova, A. T., Y. Ishii, …, R. Tycko. 2002. A structural model for Alzheimer's β-amyloid fibrils based on experimental constraints from solid state NMR. *Proc. Natl. Acad. Sci. USA.* 99:16742–16747.

43. Minton, A. P., G. C. Colclasure, and J. C. Parker. 1992. Model for the role of macromolecular crowding in regulation of cellular volume. *Proc. Natl. Acad. Sci. USA.* 89:10504–10506.

44. Paravastu, A. K., R. D. Leapman, …, R. Tycko. 2008. Molecular structural basis for polymorphism in Alzheimer's β-amyloid fibrils. *Proc. Natl. Acad. Sci. USA.* 105:18349–18354.